

# Mapping of the freshwater lens in a coastal aquifer on the Keta Barrier (Ghana) by transient electromagnetic soundings

Lars Nielsen \*, Niels O. Jørgensen, Peter Gelting

*Geological Institute, University of Copenhagen, Øster Voldgade 10, DK-1350 Copenhagen K, Denmark*

Received 18 October 2005; accepted 2 July 2006

---

## Abstract

We present a model of the freshwater lens and saltwater intrusion in a 1000m wide and 2500m long portion of the Keta Barrier, Ghana, based on 96 transient electromagnetic (TEM) measurements. Saltwater intrusions from the Gulf of Guinea to the south of the barrier and from the Keta Lagoon to the north threaten the freshwater resources. The freshwater resources are essential for supporting the relatively large population and intensive farming on the Keta Barrier. It is therefore of utmost importance to identify and map the saltwater intrusion in order to get an overview of the remaining freshwater resources. The sedimentary column below the barrier is characterised by sand and gravel deposits with layers of clay and silt. The electrical resistivity of the subsurface is most likely primarily controlled by the salinity of the pore water. The TEM method is well suited for mapping the depth to and the resistivity of good conductors, and, therefore, a strong tool for identifying the top of the low-resistivity sediments which are saturated with saline pore water. The surface marking the top of the salt-water-saturated sediments has a saucer-like shape. It is situated at 0–5 m depth close to the shorelines of the Gulf of Guinea and the Keta Lagoon, whereas it is situated at up to ~40–45 m depth in the central parts of the barrier. The freshwater lens is thin (0–5 m) close to the coasts of the Gulf of Guinea and the lagoon, whereas it may be up to ~20 m thick in the central parts of the Keta Barrier. We interpret the existence of a mixing zone with brackish water between the freshwater lens and the layers with saline pore water. This mixing zone varies in thickness from 0–5 m close to the coastlines to ~10–20 m in the central part of the barrier.

© 2006 Elsevier B.V. All rights reserved.

**Keywords:** Transient electromagnetic method; Groundwater; Freshwater lens; Saltwater intrusion; Ghana

---

## 1. Introduction

The Keta Barrier forms part of the Volta River estuary and outlet in the Atlantic Ocean in southeast Ghana (Fig. 1) and separates the Keta Lagoon to the north from the Gulf of Guinea to the south. The barrier is approximately 25 km long and has a lateral extension that varies between 1 km and 3 km. The topography of

the barrier rises to a maximum of approximately 7 m above sea level in the central portions and gradually flattens out to the lagoon side. A narrow dune field borders the coastline to the Atlantic Ocean.

The barrier lies within the dry equatorial climatic regime, the Ghana–Togo dry zone (Dickson and Benneh, 2001). The annual average temperature is 28 °C, with a minimum in August of 23 °C and a maximum of 32 °C in March. The rainfall distributions show a bimodal pattern due to the annual movement in the inter-tropical convergence zone and related shifts in

---

\* Corresponding author.

E-mail address: [ln@geol.ku.dk](mailto:ln@geol.ku.dk) (L. Nielsen).

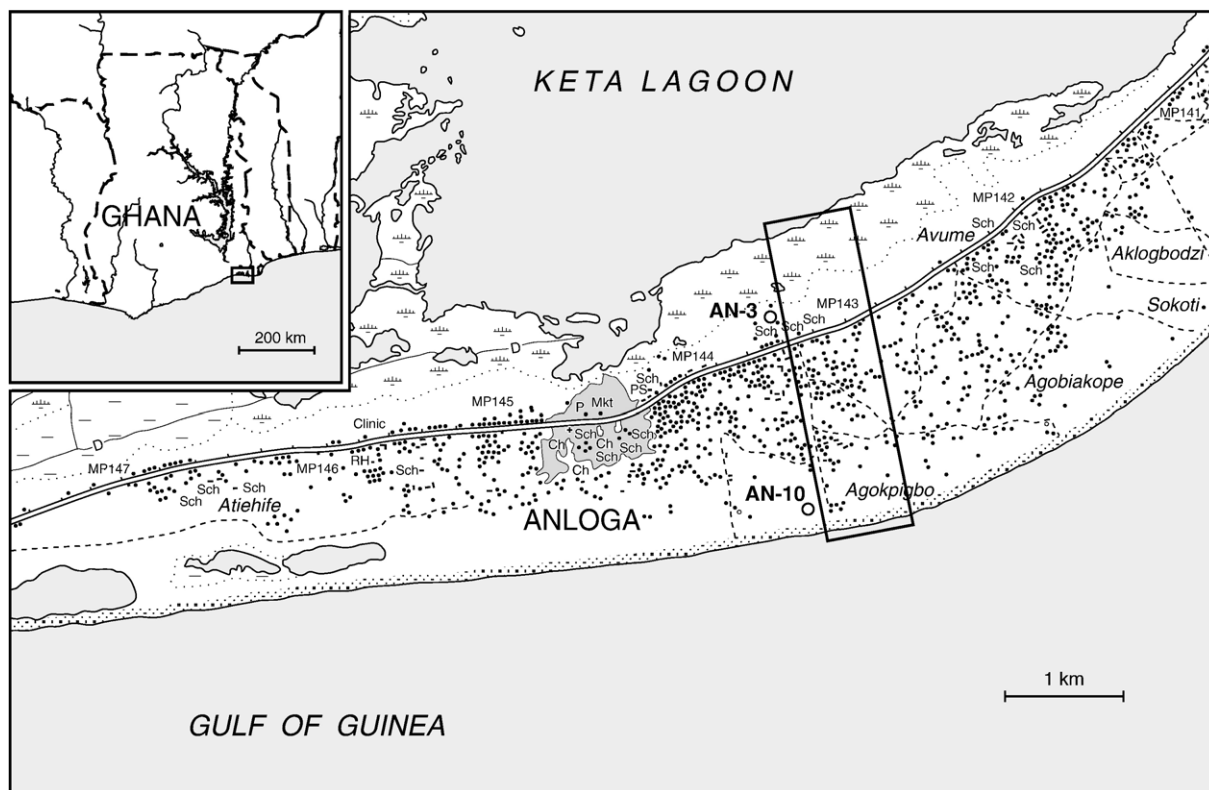


Fig. 1. Map of the Keta Barrier. Rectangle indicates the study area. The positions of wells AN-3 and AN-10 from which sedimentological logs have been constructed are shown on the map. Small dots mark positions of houses on the barrier. Typically, at least one or several small wells from which the farmers pump freshwater are found for each house.

wind directions with a major rainy season between April and July and a second season between September and November. The mean annual precipitation is between 740 mm and 890 mm and the humidity varies from 60% in the dry season to about 75% in the rainy seasons (Ojo, 1977). The precipitation often occurs in connection with squalls travelling from east to west; resulting rainfall intensities can therefore be high, sometimes more than 200 mm/h (Ojo, 1977). The mean number of rainy days for the area is approximately 70. Less is known about evaporation, potential and actual evapotranspiration. However, values for potential evapotranspiration of approximately 1300 to 1600 mm are indicated by Ojo (1977), Adu and Asiamah (1992), and Awadzi (2003), meaning that there is a deficit in the annual water balance. The actual evapotranspiration therefore heavily depends on type of vegetation and irrigation.

The socio-economic activities in the area are based on intensive vegetable farming and fishing. The population has increased dramatically over the last two decades and has led to an increase in the agricultural activity. Furthermore, an increasing number of shallow mechanized wells have been established to facilitate

sprinkling irrigation of the farmland in the central part of the sand spit. The construction of mechanized irrigation may increase the groundwater abstraction resulting in overexploitation and disturbance of the fragile equilibrium between the freshwater and the saline natural waters in the lagoon, the sea and the brackish water in the subsurface. The rapid expansion of farmland and growing population have resulted in increased consumption and demand of water for irrigation and domestic water supply putting a pressure on the limited groundwater available from the shallow aquifer. These factors are threatening the sustainability of the system.

In recent years, the transient electromagnetic (TEM) method has been extensively used in hydrogeophysical surveys, including the search for groundwater resources (e.g. Auken et al., 2003; Danielsen et al., 2003). The TEM method is an effective geophysical tool to map the depth to and the resistivity of geological layers with good electrical conductivity. Salt-water-saturated sediments normally constitute good electrical conductors, and, therefore the TEM method is well suited for mapping the transition from freshwater-saturated sediments to sediments saturated by saline pore water (e.g.

Kafri and Goldman, 2005). The aim of this paper is to map the extent of the freshwater lens and to determine the freshwater–saline water interface by use of TEM measurements in order to facilitate an evaluation of the freshwater resources in the study area on the Keta Barrier. The threats to the system and measures to be taken to ensure its sustainability are discussed.

## 2. Geology and hydrogeology of the study area

The Keta Barrier forms part of the Keta Basin, a vast coastal sedimentary basin of southeast Ghana (Akpali, 1978). The stratigraphic sequence includes Recent to Devonian rocks resting on a crystalline basement. Water-supply borehole data from the Keta area typically show an upper ~30 m interval of Recent to Pleistocene coastal deposits of unconsolidated gravel, sand and clay and a Neogene non-marine sedimentary sequence from ~30 m to ~90 m mainly made up of unconsolidated to semi-consolidated limonitic argillaceous sands with intercalating gravelly beds. The Neogene sequence rests unconformably on Eocene–Upper Cretaceous marine sediments consisting of clay, shale, glauconitic sandstone and a fractured limestone generally described as the Keta Limestone. The Keta Limestone Formation dips to the southwest ranging in depth from near surface in the republic of Togo to more than 300 m in the southwestern parts of the Keta Basin where the study area is situated. The groundwater in the Keta Limestone has been exploited since the 1960's for municipal water supply systems and is the most important deeper aquifer in the Keta Basin. The static water level of the limestone aquifer at the Keta Barrier is 2–4 m above sea level and the estimated potential yields for wells in the limestone range from c. 15 m<sup>3</sup>/h to more than 250 m<sup>3</sup>/h based on initial test pumping results during the construction of the boreholes (Bannerman, 1994).

The study area is located across the barrier east of the township Anloga (Fig. 1). The barrier is approximately 3 km wide at this location. In the vicinity of Anloga, the Keta Limestone is recorded at a depth of c. 200 m in a water borehole from the beginning of the 1960s. The well log of this borehole confirms the occurrence of an overlying siliclastic sedimentary sequence of unconsolidated gravel, sand and intercalating clay layers. However, the groundwater in the deeper permeable parts of the siliclastic sequence has not been exploited due to the risk of enhanced electrical conductivity and seawater intrusion. Thus, saline groundwater is encountered at <100 m depth in abounded water wells in the central portion of the barrier in the study area. Most wells for local domestic water supply and agricultural

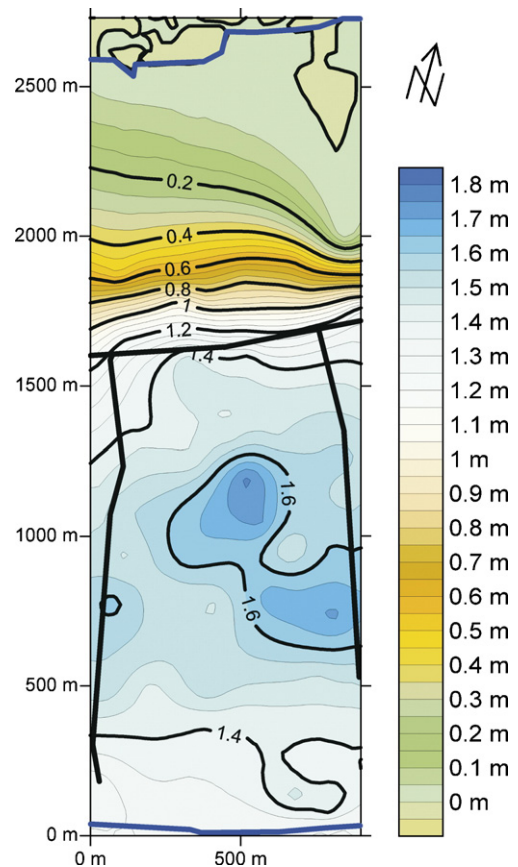


Fig. 2. Groundwater potential based on the numerous shallow wells scattered throughout the study area. Values are in metres.

purpose are dug wells and boreholes less than 10 m deep and established in the unconfined top part of the shallow aquifer comprising Recent to sub-Recent near-coastal marine sediments. Yields in the order of 7–9 m<sup>3</sup>/h have been recorded in the aquifer (Kortatsi and Agyekum, 1999). The groundwater potential in the shallow aquifer reveals an annual fluctuation of approximately 1 m, depending on the amount of recharge in the rainy seasons. The static water level reaches a maximum of approximately 2 m above sea level in the central part of the barrier (Fig. 2).

Well logging of shallow monitoring boreholes (<35 m) in the dune field at the seaside and the lagoon side of the barrier confirms a lithological succession of sand and silt with some intercalations of gravel and clay and more substantial clay and silt layers at a depth of approximately 31–35 m at the seaside portion of the barrier (Fig. 3) (see also Kortatsi and Agyekum, 1999). The fringe of the lagoon is covered by saline clayey marshy soil. Scattered outcrops of a 10–20 cm thick peat layer are observed at the lagoon fringe and are also observed in shallow monitoring boreholes established

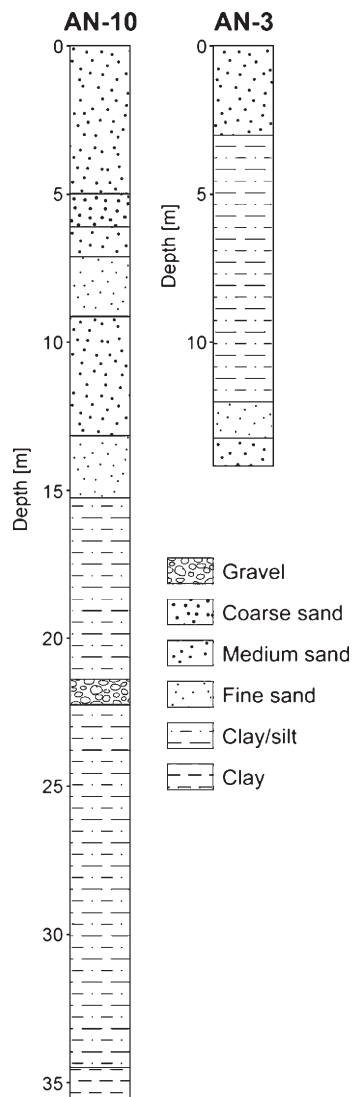


Fig. 3. Sedimentological log from the study area. The positions of the wells are indicated in Fig. 1. The log is dominated by different types of sand. Minor amounts of clay, silt and gravel are also present.

in the farm land. The lithological succession at the lagoon side consists of medium to fine sand intercalated with silt and clay layers (Fig. 3). The sedimentary sequences observed are consistent with the general model of the sedimentary environment and the wedge-shaped structure of a transgressing barrier–lagoon system, which represents the growth and migration of barriers over their fine-grained back-barrier deposits (Kraft et al., 1987; Reinson, 1992).

Saline groundwater is encountered at < 100 m depth in abounded water wells in the central portion of the barrier. This aquifer may be considered as being semi-confined according to the occurrences of several clay layers in the deeper part of sedimentary sequence. At the present time

there is no functioning borehole screened in the Keta Limestone Formation within or close to the study area.

### 3. Methodology

The freshwater–salt water transition zone below the barrier is expected to constitute a marked change in electrical resistivity from relatively high resistivities in the shallow freshwater zone to relatively low resistivities in the deeper sediments, which are saturated by salt water. We use the transient electromagnetic (TEM) method to map the depth to the freshwater–salt water transition.

The TEM method is well suited for mapping the depth to and the conductivity of highly conductive material in the subsurface, and it was originally developed for mapping mineral deposits in the 60s and 70s (e.g. Spies and Frischknecht, 1991; Fountain, 1998). The resistivity contrasts between such mineralizations and the host rock are typically very large, and therefore the TEM method is ideal for locating the mineral deposits. Since the 1980s the development of new instrumentation and interpretation methods has further refined the TEM method and allowed for the mapping of groundwater reservoirs in clastic sediments (e.g. Fitterman and Stewart, 1986; Mills et al., 1988; McNeill, 1990). In such integrated hydrogeological–geophysical studies, the resistivity contrasts that need to be resolved by the TEM method are significantly lower than in the case of locating mineral deposits.

Numerous hydrogeological–geophysical TEM mapping studies and model resolution tests based on least squares inversion of the acquired data have shown that the TEM method is well suited for resolving the coarse-grained resistivity structure of the upper 100–300 m of the subsurface, depending on the configuration and specifications of the employed TEM equipment as well as the resistivity structure of the subsurface (Danielsen et al., 2003; Sørensen and Auken, 2004). Typically, a one-dimensional (1-D) layered resistivity model consisting of 3–5 layers can be resolved for the uppermost ~ 100 m of the subsurface from a single TEM sounding. Samples from the very few wells with significant penetration depths of up to 32 m that have been drilled on the Keta Barrier indicate that the sedimentary sequence consist of alternating, silt-, sand-, and gravel-rich deposits with thin intercalating clay horizons, which are interpreted to have been deposited in dynamic barrier–lagoon systems (Fig. 3; Gelting, 2004). The individual lithological units identified in the wells are typically no more than a few metres thick. Based on the lithological borehole data, we expect the hydrological conductivity to be relatively high



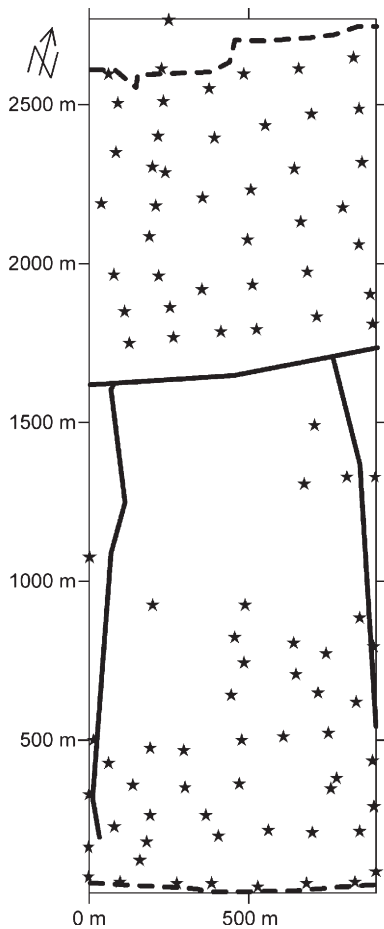


Fig. 4. Map of the study area showing the positions of the TEM soundings used in the geophysical mapping (stars). Bold lines indicate main roads. Shorelines at the lagoon and the Gulf of Guinea are shown with dashed lines.

in the bulk part of the sedimentary column. Numerous resistivity contrasts may occur on a short scale. However, we find it most likely to assume that the large-scale resistivity contrasts, which can potentially be resolved by the TEM soundings, are mainly controlled by the freshwater–salt water transition, which is believed to be located within the uppermost 100 m of the subsurface everywhere on the Keta Barrier (Kortatsi and Agyekum, 1999).

We use the Protem 47 instrument (Geonics Ltd.) with a 40 m by 40 m transmitter loop and a receiver coil in the centre. This instrumentation setup has been successfully used in numerous integrated hydrogeological–geophysical studies aimed at mapping groundwater reservoirs since the 1980s. In our system setup the turn-off time for the transmitter current was set to 2.5  $\mu$ s. Over this time interval the transmitter current was gradually (approximately linearly) turned off. This relatively short turn-off

time allows for a proper description of the resistivity properties of the uppermost parts of the subsurface. The decay of the secondary magnetic field recorded by the receiver coil was sampled over three segments as this is the only way the instrument can handle the dynamic range of the received signal: ultra high (237.5 Hz), very high (62.5 Hz), and high (25 Hz). For each segment, measurements have been made in 20 time windows (gates). The ultra high segment samples the signals for recording times of 7  $\mu$ s to 700  $\mu$ s, the very high segment covers the 35  $\mu$ s to 2.8 ms time interval, whereas the high segment samples the 88  $\mu$ s to 7 ms time interval. Initial noise tests showed that the signal-noise level was unusually high in the study area. Relatively low transmitter currents of 0.5–1.0 A were selected for the ultra high segment in order to avoid measurements falling outside the dynamic range of the recording instrument. For the very high and high segments a standard transmitter current of 3 A was used.

#### 4. Results

A total of 98 TEM soundings were conducted in the study area (Fig. 4). The central part of the study area is

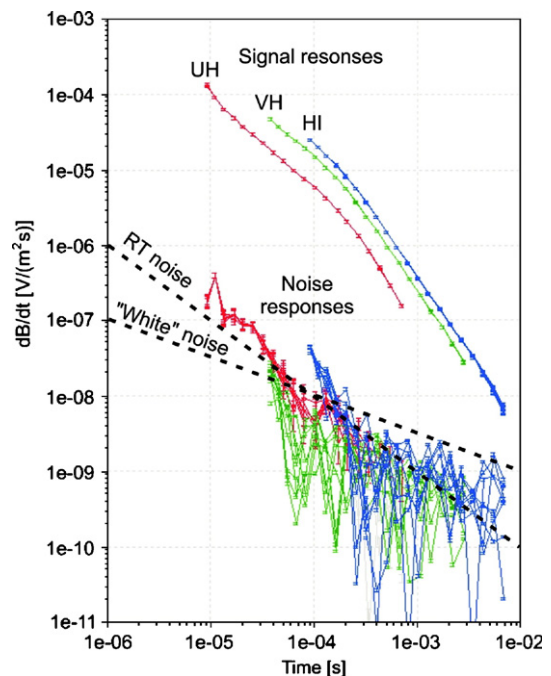
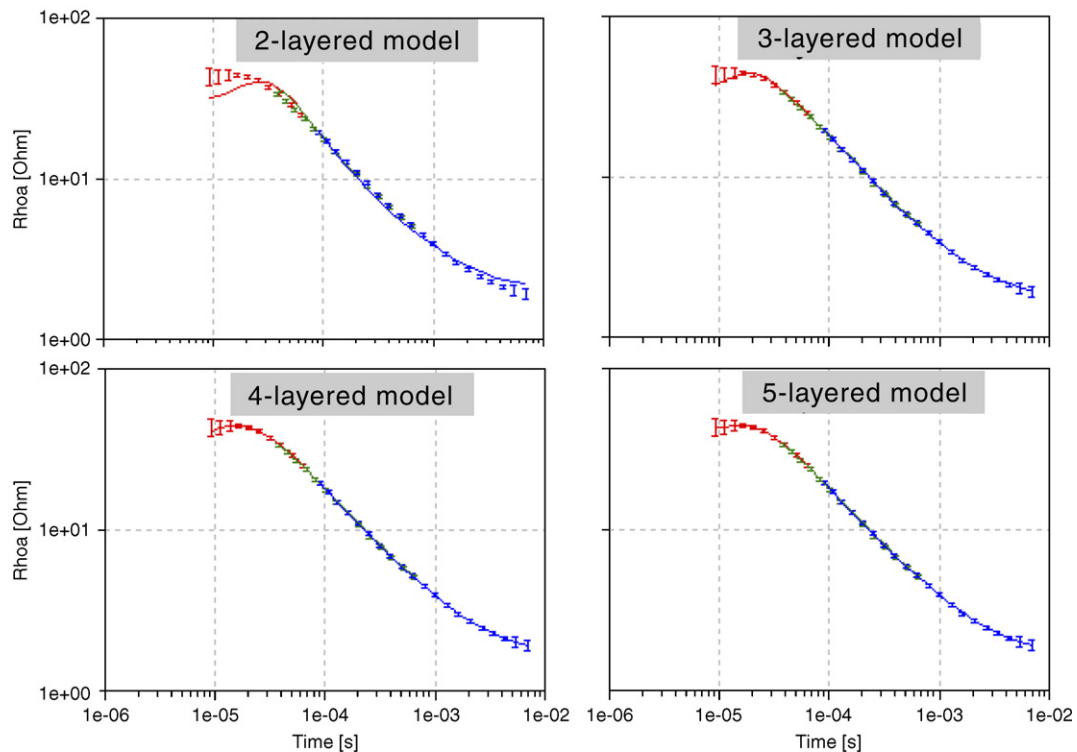


Fig. 5. Signal and noise responses measured for the ultra high (UH), very high (VH), and high (HI) segments. The colour used for the TEM response in a given time segment corresponds to that for noise values measured in the same time segment. Theoretical curves for “white” noise and noise generated by radio transmitters (RT) are shown with dashed lines.

more sparsely covered than the northern and southern-most parts due to the relatively dense infrastructure of the central part. Tests showed that a minimum distance of 150m had to be kept between the points of measurement and conductive installations (e.g. power cables) in order to avoid severe noise effects. A representative example of measured signals and noise tests for the three recording segments is shown in Fig. 5. A power law distribution is assumed for the noise model (cf. Munkholm and Auken, 1996). The level of the “white noise” is proportional to  $t^{-1/2}$ . The level of the noise generated by radio transmitters is modelled to

decrease faster. Note that, in general, the signal response is significantly stronger than the background noise level. Only the latest times covered by the high segment seem to be significantly affected by the noise. The high signal-to-noise ratio, which is typically obtained, is interpreted to be a result of the combined effects of the very few cultural noise sources in the areas where measurements have been conducted and the response of a shallow geological feature with high electrical conductivity. The different signal levels recorded for the individual segments are accounted for during the inversion process used for deriving the subsurface resistivity structure.



Resolution test, 3-layered model

	Resistivity	Thickness	Depth	ResSTD	ThkSTD	DepSTD
Layer 1	36.5	24.6	24.6	1.03	1.02	1.02
Layer 2	2.4	11.4	36.0	1.09	1.06	1.03
Layer 3	1.0			1.04		

Resolution test, 4-layered model

	Resistivity	Thickness	Depth	ResSTD	ThkSTD	DepSTD
Layer 1	39.4	22.0	22.0	1.08	1.11	1.11
Layer 2	4.4	8.2	30.2	1.72	1.16	1.09
Layer 3	1.4	11.2	41.4	1.21	1.25	1.10
Layer 4	0.9			1.06		

Fig. 6. Apparent resistivity data and model response curves for two-, three-, four-, and five-layered models (top). Model parameter values and the corresponding model resolution values for the three- and four-layered models are shown below. Resistivities are in ohm-metres, and thicknesses and depths are given in metres. ResSTD, ThkSTD, and DepSTD are the estimated relative standard deviations of resistivity, thickness, and depth values.

Initial data processing of the TEM data, i.e. editing of data and assignment of a priori uncertainties, was made with the SiTEM programme. Subsequently, the TEM data were inverted to obtain 1-D resistivity models of the subsurface with the SEMDI programme. The SiTEM and SEMDI programmes were developed by the HydroGeophysics Group, Aarhus University (Munkholm and Auken, 1996; Effersø et al., 1999).

The inversion procedure relies on an iterative least squares algorithm, which requires a starting model. A major advantage of least squares-based inverse methods is that they provide measures of model resolution (e.g. Auken et al., 2002). Here, the model resolution estimates for individual model parameters are given in relative numbers. Ideally, a model parameter should have a resolution value of 1.00. A resolution value of 1.05 indicates an estimated uncertainty of 5% of the corresponding model parameter. In general, layers with low resistivities are well resolved by the TEM method, whereas highly resistive layers (resistivities of  $\sim 100 \Omega\text{-m}$  and more) are poorly resolved. For each inversion an a priori model is defined. A crucial step in the definition of the starting model is the choice of the number of layers to be included in the model. This number cannot be changed automatically by the inversion algorithm. We seek the model with the smallest number of layers which can provide a satisfactory fit to the measured data. A simple model will be better resolved by the inversion procedure than a model containing a larger number of layers. A modelling example is outlined in Fig. 6. For the given data set, two-, three-, four-, and five-layer models are tested. The fit to the data for the four models is shown in Fig. 6 (top). In all four cases the iterative inversion procedure has converged, and further iterations do not lead to further significant changes to the models and the fit to the data. The two-layered model provides a relatively poor fit to the data, and the misfits show a systematic behaviour. For early recording times, the modelled curve systematically shows lower values than the observed data, and for the latest recording times the modelled curve shows values which are systematically too large. The three-, four-, and five-layered models all fit the data within the specified error bars and do not show significant systematic misfits. The fit to the data provided by the four- and five-layered models are basically identical. The response of the three-layered model provides a slightly poorer misfit to the first three data points. However, the modelled curve falls within the relatively large error bars expected for this part of the ultra high segment, and do not seem to be too significant. Thus, the simplest model, which provides a satisfactory fit to the data, is the three-layered model.

The model resolution test provided by the inversion algorithm for the three- and four-layered models is shown in Fig. 6 (bottom). The model parameters of the three-layered model are well resolved by the inversion procedure. None of the estimated relative uncertainties are larger than 1.09. For the four-layered model, the estimated uncertainties of the resistivities of layers 2 and 3 as well as the thickness of layer 3 are significantly larger. Thus, the model parameters of the four-layered model are relatively poorly constrained by the data. Therefore, in this case, the three-layered model is preferred. Similar investigations of data fit and model resolution tests for different model types have been made for each of the TEM soundings made in the study area. Typically, a total of about 10 iterations are required before a satisfactory fit to the observed data is obtained and the model has converged, depending on how far the

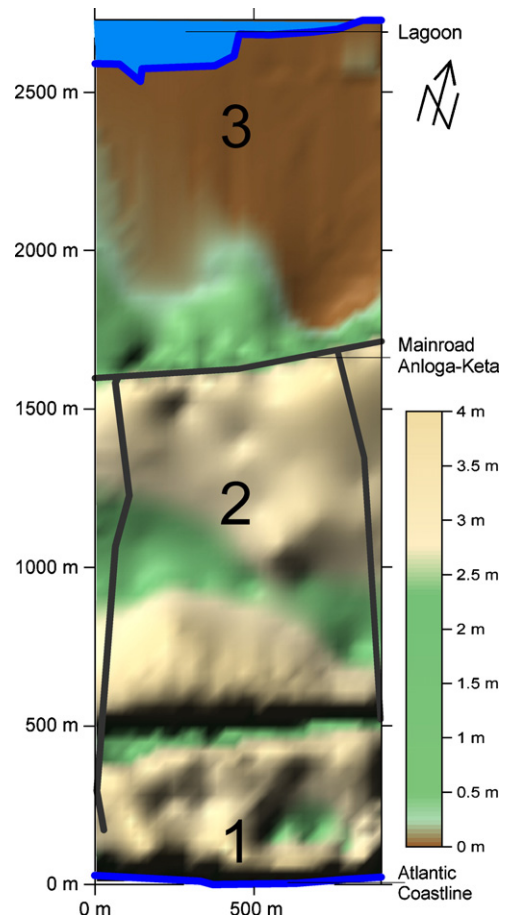


Fig. 7. The study area is divided into three parts: 1) The coastline at the Atlantic Ocean (Gulf of Guinea); 2) the central part from the coast of the Atlantic Ocean to the main road (Anloga-Keta); and 3) the area between the main road (Anloga-Keta) and the lagoon. Topographic elevations are relative to the mean sea level of the Atlantic Ocean.

model parameter values of the starting model are from the model parameter values of the final model found by the iterative inversion procedure.

## 5. Resistivity models and hydrogeological implications

The study area is divided into three different parts on the map of Fig. 7. Interpretation of the TEM soundings results in characteristic resistivity models for the individual parts of the study area. We assume that the sandy formations intercalated with silt and clay layers as observed in the boreholes are representative for all three parts of the study area.

The TEM soundings conducted close to the Gulf of Guinea in the southernmost part of the study area can be explained by simple two-layered models. The resistivity of the top layer varies between 8 and 33  $\Omega$ -m while it is only 0.9–1.2  $\Omega$ -m in the bottom layer. The boundary between the two layers is found at 6 to 16 m depth. A representative data example and the corresponding inversion result are shown in Fig. 8. The model parameter values are well constrained by the data with relative uncertainties varying between 1.01 and 1.07.

The rather low resistivities of 8 to 33  $\Omega$ -m indicate that the pore water of the top layer may to some extent be brackish or that this layer is rich in clay. We interpret the layer boundary between the two layers to mark the transition from fresh or brackish pore water in the top of the sedimentary column to saline pore water in the bottom.

In the central part of the study area, three- and four-layered resistivity models are required in order to obtain satisfactory fits to the TEM data (Figs. 9 and 10). The topmost layer is characterised by relatively high resistivities of  $\sim 20$ –70  $\Omega$ -m. The highest of these resistivity values ( $>60$   $\Omega$ -m) are relatively poorly constrained by the data because of the difficulties of the TEM method concerning estimation of high resistivities (Fig. 9). However, the lower resistivity values ( $<50$   $\Omega$ -m) of the top layer are relatively well constrained by the data with estimated relative uncertainties of  $\sim 1.10$ –1.15 (Fig. 10). The rather low resistivity values of less than 50  $\Omega$ -m of some parts of the top layer may indicate a significant clay content or possibly the presence of brackish pore water. The thickness of the top layer gradually increases from around 4–8 m near the coast of the Gulf of Guinea to

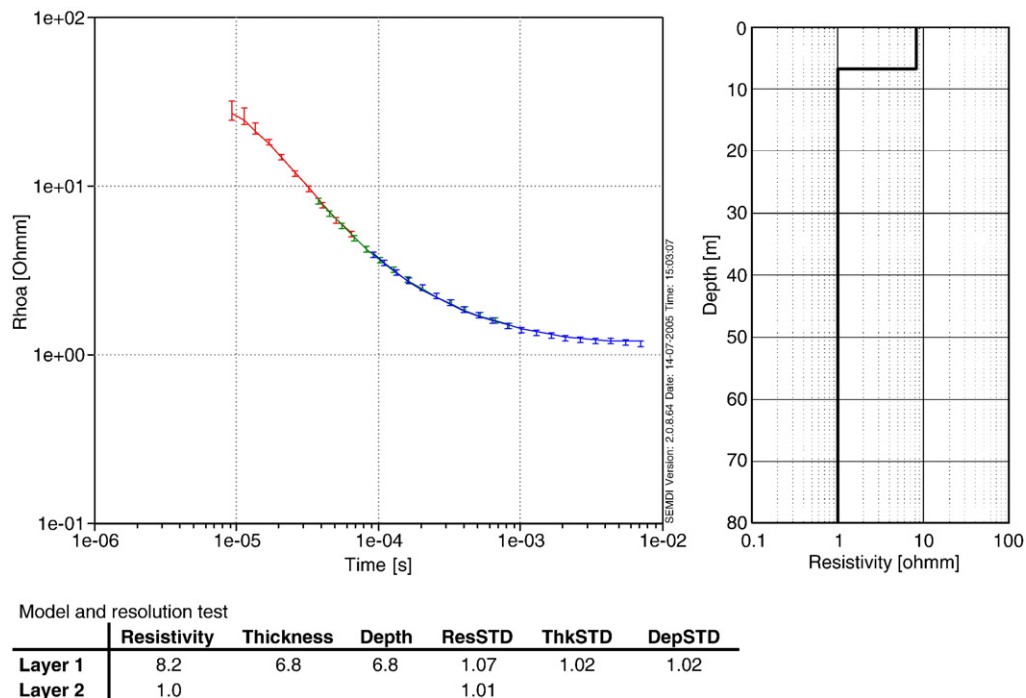


Fig. 8. Representative apparent resistivity data (shown with error bars) and a two-layered model from part 1 of the study area (see Fig. 7). The model response of the two-layered model is shown with a solid line. Different colours in the data plot indicate ultra high, very high and high segments (see Fig. 5). Data have been processed to form a continuous line. Below, model parameters and relative model resolution estimates of the two-layered model are shown. Resistivities are in ohm-metres, and thicknesses and depths are given in metres. ResSTD, ThkSTD, and DepSTD are the estimated relative standard deviations of resistivity, thickness, and depth values.



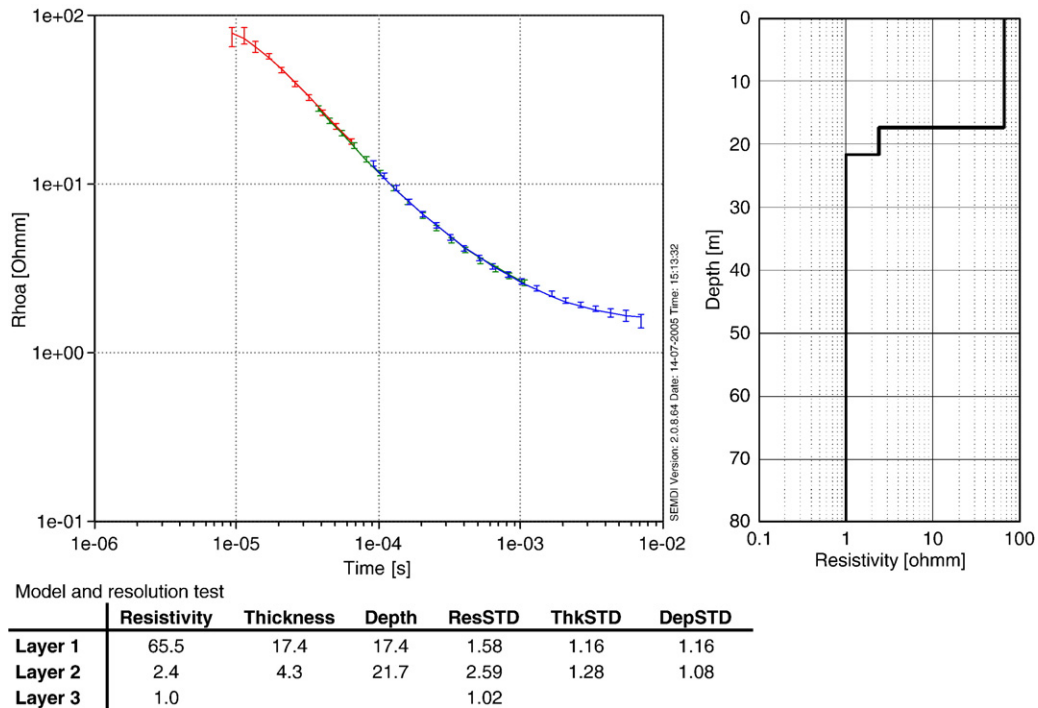


Fig. 9. Representative apparent resistivity data (shown with error bars) and a three-layered model from part 2 of the study area (see Fig. 7). The model response of the three-layered model is shown with a solid line. Different colours in the data plot indicate ultra high, very high and high segments (see Fig. 5). Data have been processed to form a continuous line. Below, model parameters and relative model resolution estimates of the three-layered model are shown. Resistivities are in ohm-metres, and thicknesses and depths are given in metres. ResSTD, ThkSTD, and DepSTD are the estimated relative standard deviations of resistivity, thickness, and depth values.

~20m in the central part of the Keta Barrier. Below the top layer, we find one or two layers with resistivities between 1.2 and 7.9  $\Omega$ -m (average resistivity ~2.5  $\Omega$ -m). The total thickness of this or these layers amounts to ~4m close to the Atlantic coast, while it is around 24m in the central part of the barrier. The second layer or second and third layers are most well constrained by the inversion in the central part of the barrier, where this layer/these layers are thickest. At the bottom of the models for the central part of the study area, we find a low-resistive layer with resistivities of 0.9–1.0  $\Omega$ -m. The depth to this layer is only 8–10m in the vicinity of the Atlantic coast line whereas it is up to ~40–45m in the central part of the Keta Barrier. The top layer of relatively high resistivity is, again, interpreted as representing the freshwater zone, and the bottom layer of low resistivity is interpreted as the zone with saline pore water. We interpret the second or second and third layers of intermediate resistivity to represent a mixing zone of brackish pore water.

In the northern part of the study area (Fig. 7), the TEM soundings are interpreted by four-, three-, and two-layered models. Just north of the main road to

Anloga, the data require a four-layered resistivity structure (Fig. 11). This model type is very similar to the three-layered models found in the central part of the Keta Barrier, except that it includes a very thin low-resistive top layer above a layer of relatively high resistivity. The top layer is not well constrained by the inversion, because of its limited thickness (probably <2m). However, the trend of the data curve indicates the existence of the layer. The thin low-resistive top layer may be attributed to hyper saline pore water brought to this part of the barrier by flooding events from the lagoon to the north. Salt flake deposits found on the surface of the northern part of the study area support this hypothesis. The inversion procedure estimates low to moderately high relative uncertainty values for the second layer, which has a relatively high resistivity. The parameters of the low-resistive layers three and four are well constrained. The layer of relatively high resistivity is again interpreted as a zone with fresh pore water, whereas layers three and four are interpreted as being representative of a mixing zone and a zone with saline pore water, respectively. Towards the lagoon, the resistivity of the high-resistive

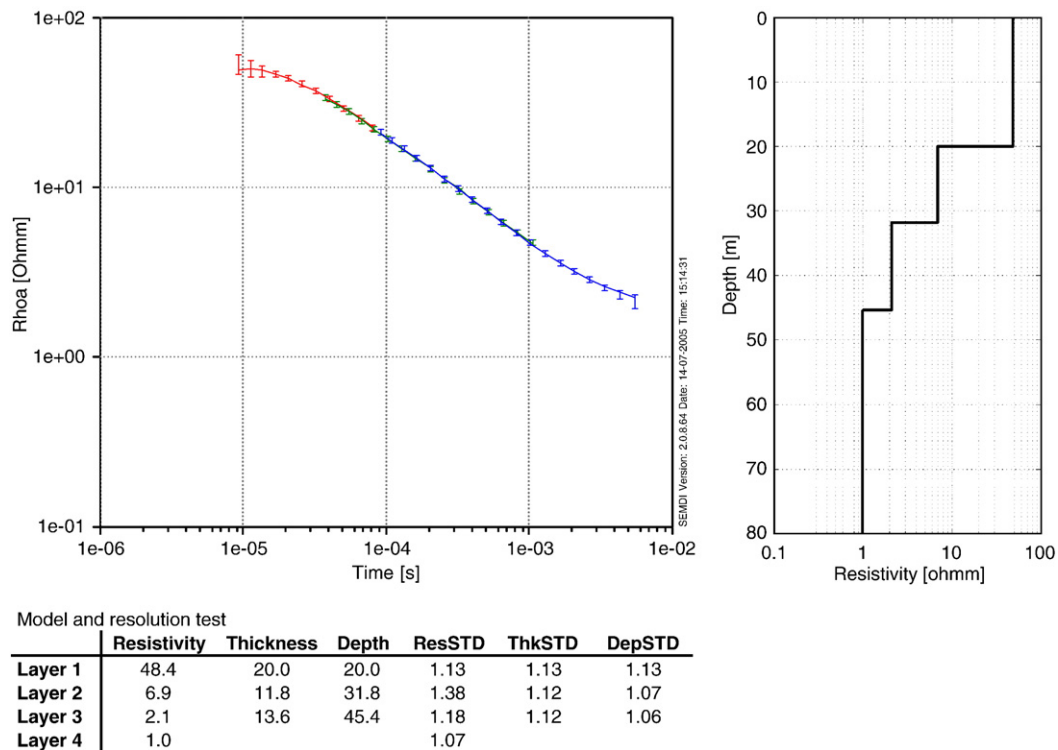


Fig. 10. Representative apparent resistivity data (shown with error bars) and a four-layered model from part 2 of the study area (see Fig. 7). The model response of the four-layered model is shown with a solid line. Different colours in the data plot indicate ultra high, very high and high segments (see Fig. 5). Data have been processed to form a continuous line. Below, model parameters and relative model resolution estimates of the four-layered model are shown. Resistivities are in ohm-metres, and thicknesses and depths are given in metres. ResSTD, ThkSTD, and DepSTD are the estimated relative standard deviations of resistivity, thickness, and depth values.

layer gradually decreases, and the boundary between layers three and four diminishes. On the edge of the lagoon the data can be interpreted by a two-layered structure consisting of two low-resistive layers interpreted to represent a zone of hyper saline pore water on top of the salt-water-saturated sediments.

Fig. 12 shows cross sections, which outline our interpretation of the state of the pore water based on the TEM soundings. Three-dimensional views of the interpreted depths to the surfaces representing the top of the freshwater lens, the top of the mixing zone, and the top of the salt-water-saturated sediments are shown in Fig. 13. The freshwater lens is thin (0–5 m) close to the coasts of the Gulf of Guinea and the lagoon. In the central parts of the Keta Barrier, the freshwater layer is up to ~20 m thick. Overall, the top of the salt-water-saturated sediments has a shape like the cross section of a saucer. It is situated at 0–5 m depth close to the shorelines of the Gulf of Guinea and the lagoon, whereas it is situated at up to ~40–45 m depth in the central parts of the barrier. The interpreted mixing zone with brackish water between the freshwater lens and the

top of the saline layer varies in thickness from 0–5 m close to the coast lines to ~10–20 m in the central part of the barrier. Thus, the mixing zone seems to be well developed in the central parts of the barrier, whereas it may be very thin or even absent in some parts of the study area close to the shore lines of the Gulf of Guinea and the lagoon.

## 6. Discussion

Our interpretation of the freshwater–salt water transition based on the TEM recordings may, at least partly, be obscured by unknown large-scale lithological changes such as possible transitions from sand/silt-rich deposits in the upper part of the investigated depth interval to clay-rich deposits in the deeper parts. However, it is very difficult to explain the very low resistivities of less than  $2 \Omega\text{-m}$  that are found in the deep parts of the 1-D resistivity models without assuming that the sediments to a large degree are saturated by pore water of high salinity. Further, current sedimentary models developed for the formation and development of barrier–lagoon type

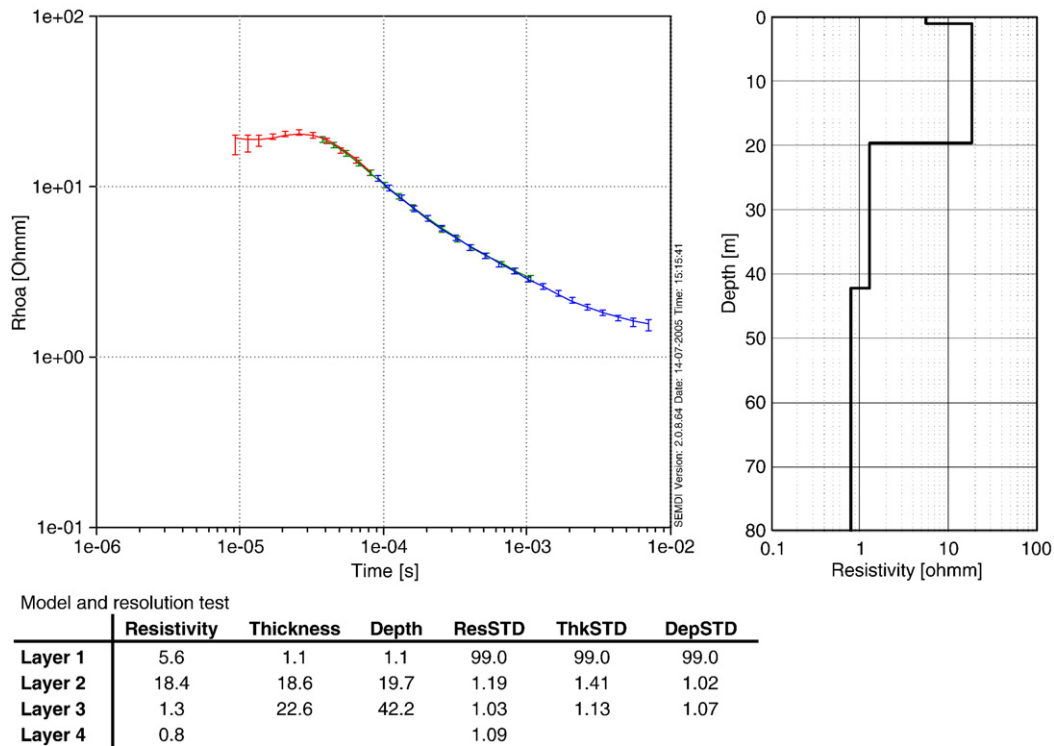


Fig. 11. Representative apparent resistivity data (shown with error bars) and a four-layered model from part 3 of the study area (see Fig. 7). The model response of the four-layered model is shown with a solid line. Different colours in the data plot indicate ultra high, very high and high segments (see Fig. 5). Data have been processed to form a continuous line. Below, model parameters and relative model resolution estimates of the four-layered model are shown. Resistivities are in ohm-metres, and thicknesses and depths are given in metres. ResSTD, ThkSTD, and DepSTD are the estimated relative standard deviations of resistivity, thickness, and depth values.

environments of the same type as the Keta Barrier do not include a thick clay layer at 20–50 m depth with a saucer-like shape centred below the central parts of the barriers (e.g. Kraft et al., 1987; Reinson, 1992).

We assess the validity of our resistivity models based on analysis of data fit and model resolution. The model resolution values provided by the inversion are representative only for subsurface structures that can be captured by the type of model parametrization on which the inversion algorithm relies. If the subsurface structures deviate significantly from these assumptions (e.g. deviations from one-dimensionality and layer boundaries being transition/gradient zones rather than sharp boundaries) then the estimated model uncertainties are too optimistic. Goldman et al. (1994) showed that 3-D structures may cause artificial low resistivities at depth in 1-D inversion results. However, we consistently observe the low-resistive layer, which we interpret to reflect salt-water-saturated sediment, over the entire study area. Therefore, we do not expect that this low-resistive layer can be caused solely by 3-D effects.

Kafri and Goldman (2005) use electromagnetic data and Archie's law (Archie, 1942) to estimate porosity in aquifers with saline groundwater. In principle, we could use Archie's law to estimate the salinity of the pore water in the study area. However, the results that can be obtained from using Archie's law are strongly dependent on the choice of material-dependent empirical factors. We have no good control of these factors in our study area mainly due to the lack of borehole information. Therefore, we have not made such estimates based on Archie's law yet.

The freshwater lens in unconfined coastal aquifers is generally described by the Dupuit–Ghyben–Herzberg theory. This theory is based on assumptions about isotropy and stationary conditions and shows that the depth to the freshwater–salt water interface is directly proportional to the elevation of the water table above mean sea level and the densities of the water bodies (Hubbert, 1940; Vacher, 1988). It is generally assumed that the freshwater lens below small islands and barriers is symmetrical about the island/barrier centre. In the central part of the study area, the groundwater

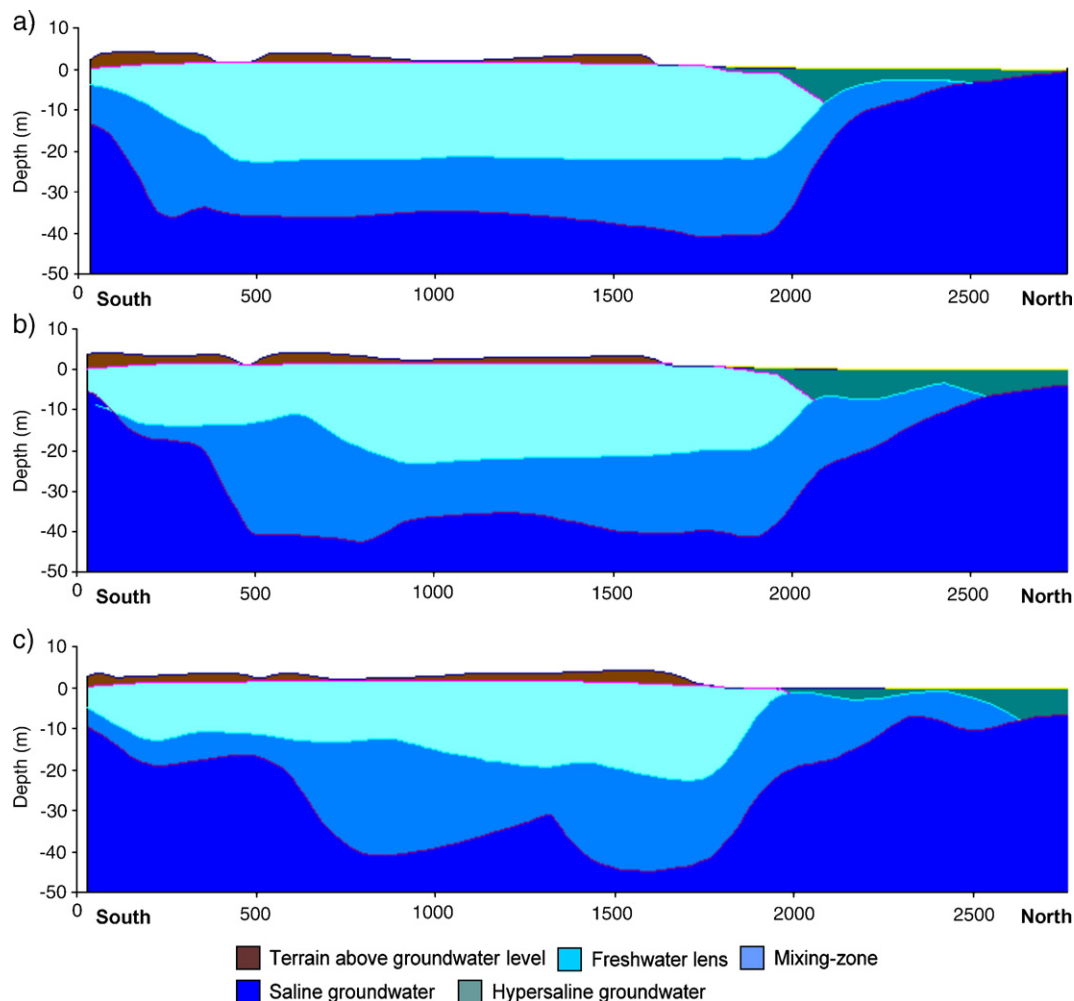


Fig. 12. Three north–south-oriented cross sections (a, b, and c). The freshwater lens, the mixing zone, the salt-water-saturated sediments, and the hyper-saline-groundwater-saturated sediments are indicated. The cross sections are from the westernmost part (a), the central part (b) and the easternmost part (c) of the study area.

potential reaches a maximum of approximately 2m above sea level (Fig. 14). Based on the Dupuit–Ghyben–Herzberg theory alone, one would expect a freshwater lens with a thickness of approximately 80m in this area. The present study indicates that the freshwater lens has a maximum thickness of about 24m in the central part of the barrier (Fig. 2), which is considerably less than expected from the Dupuit–Ghyben–Herzberg theory. It has been demonstrated that variability in hydraulic parameters and recharge may result in a freshwater lens thickness that deviates considerably from what is expected using the Dupuit–Ghyben–Herzberg theory (Vacher 1978, 1988). The pronounced variability of the depositional environments of siliciclastic barriers may strongly affect the freshwater lens morphology. Transgressive barriers

often show an ocean dipping layer of fine-grained sediments, which leads to an asymmetry of the freshwater lens, thickest on the ocean side where the clay layer is deepest (Schneider and Kruse, 2003). Furthermore, important factors that may control the geometry of the freshwater lens may be recharge, the vegetation of the terrains, groundwater abstraction and the evapotranspiration (Schneider and Kruse, 2003). We assume that the expected deviations from isotropic and stationary conditions in the study area are the main factors explaining that the maximum freshwater lens thickness found in the study area is much smaller than expected from the Dupuit–Ghyben–Herzberg theory.

The configuration of the transition zone between freshwater and the salty groundwater depends on aquifer parameters, i.e. hydraulic conductivity, porosity and the



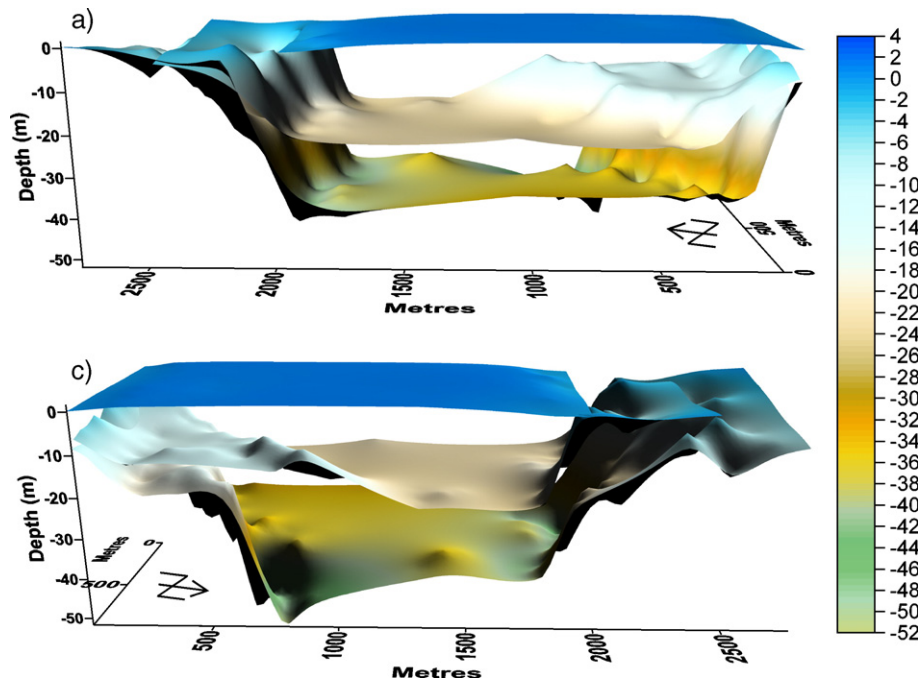


Fig. 13. Three-dimensional views of the top surfaces of the freshwater lens, the mixing zone, and the salt-water-saturated sediments. See north arrows for orientation of the two views.

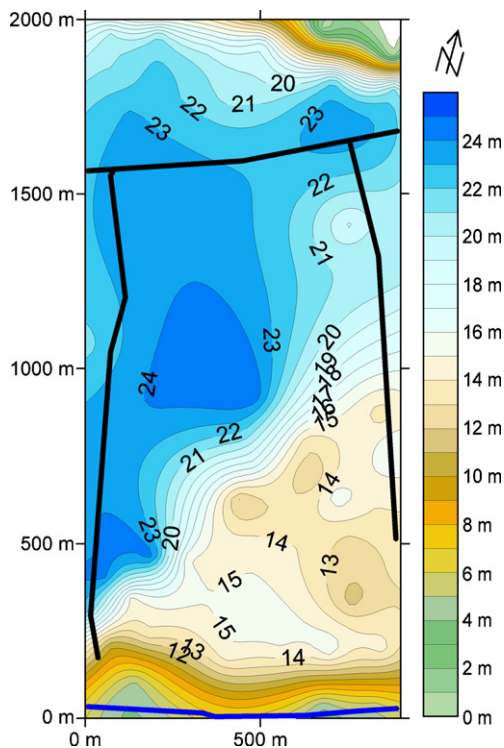


Fig. 14. Map of the thickness of the freshwater lens. Contour interval is 1 m. Solid black lines indicate main roads in the area (see Figs. 1 and 5).

hydraulic gradient (Fetter, 1993). Tidal fluctuations in the hydraulic head may also induce freshwater–salt water mixing (Cooper, 1959).

Since the 1930–40's the Keta Barrier has developed into an important zone of intensive agriculture (Armah et al., 1997; Awadzi, 2003). North of the main road, farm beds are located in a continuous belt between the main road and the salty marsh flat adjoining the lagoon (Fig. 1). South of the main road the fields are located in local artificial depressions parallel to the coast and beach ridges interspaced with higher grounds occupied by the village and single farmhouses. The farm beds are raised 15–20 cm above ground level due to the nearness of the water table to the surface. The beds are narrow varying in width from 2–3 m and generally have a length of 10 to 15 m. The beds are separated by narrow trenches, which serve as footpath and drainage channels in the rainy seasons. The production system of intensive gardening has traditionally been based on low profile irrigation using buckets and watering cans utilizing a large number of hand dug wells, mostly 1.0–1.5 m deep, located in between the farm beds and tapping the shallow groundwater aquifer in the Recent to sub-Recent sand formations. A calculation of the water balance is difficult due to the lack of solid information on the evapotranspiration and abstraction of groundwater in the study area. However, Kortatsi

and Agyekum (1999) tried to estimate the water balance in the area based on some assumption of the minimum amount of water required to irrigate the land under crop production. They concluded that equilibrium existed between recharge, groundwater abstraction and discharge to the sea and lagoon that was able to sustain the rate of groundwater abstraction for irrigation and domestic water supply at that time. Furthermore, they concluded that a further development of groundwater abstraction for intensive irrigation in the area might result in gradually increasing salinity of the shallow groundwater with a negative consequence for the crop production. However, the population has increased dramatically during the last two decades and the agricultural activity has increased. Furthermore, an increasing number of shallow mechanized wells have been established to facilitate sprinkling irrigation of the farmland in the central part of the sand spit. Potentially, the relatively thin freshwater lens with a thickness of only 24m in the central part of the study area may be threatened by increased groundwater abstraction caused by the more efficient mechanized irrigation systems. The rapid expansion of farmland and growing population have resulted in increased consumption and demand of water for irrigation and domestic water supply putting a pressure on the limited groundwater available from the shallow aquifer, thus threatening the sustainability of the system. However, drip irrigation systems have recently been introduced among a number of farmers, which in the future may result in a more sustainable use of the existing groundwater resource. Continued monitoring of the freshwater lens over a number of years could answer the question whether or not the new irrigation strategies result in a sustainable use of the groundwater resource.

## 7. Conclusions

Based on 96 TEM measurements conducted over a 1000m by 2500m portion of the Keta Barrier and hydrogeological studies we conclude that the TEM method is ideal for mapping the freshwater–salt water interface below the barrier. Unusually high signal-to-noise ratios can be obtained in the study area, and the data constrain the depth to the top of the salt-water-saturated sediments, which have a low resistivity of around 1  $\Omega$ -m, with a high degree of certainty.

The surface marking the top of the salt-water-saturated sediments below the barrier has a saucer-like shape. The saline pore water is found already at 0–5m depth close to the shorelines of the Gulf of Guinea and

the Keta Lagoon, whereas it is situated significantly deeper (~40–45m depth) in the central parts of the barrier.

The freshwater lens is only 0–5m thick close to the shorelines bounding the Keta Barrier to the north and to the south. In the central parts of the barrier, it may be up to ~20m thick. A mixing zone with brackish pore water is found between the freshwater lens and the top of the salt-water-saturated sediments. This zone has a thickness of 0–5m close to the shore lines, whereas it may be up to ~10–20m thick in the central part of the barrier.

A growing population and intensive agricultural activities threaten the remaining freshwater resources of the barrier.

## Acknowledgements

This project was funded by the DANIDA, the Danish International Development Authority, grant no 104. Dan. 8L/300. Lars Nielsen was partly funded by the Danish Natural Science Research Council. Discussions with N. B. Christiansen and E. Auken, University of Aarhus, Denmark, about collection and interpretation of TEM data are highly appreciated. The TEM data processing and inversion programmes were kindly provided by the HydroGeophysics Group, University of Aarhus. Discussions with Gunver Krarup Pedersen, University of Copenhagen, about the sedimentary characteristics of barrier-type environments are greatly acknowledged. Esben Auken, an anonymous reviewer and editor A. Hördt provided valuable comments and suggestions for adjustments.

## References

- Adu, S.V., Asiamah, R.D., 1992. Soils of the Ayensy/Densu basin, Ghana. Soil Research Institute 1992. Advent Press. 117 pp.
- Akpati, B.N., 1978. Geologic structure of and evolution of the Keta Basin, Ghana, West Africa. Geological Society of America Bulletin 89, 124–132.
- Archie, G.W., 1942. The electrical resistivity log as an aid in determining some reservoir characteristics. Transactions of the American Institute of Mining and Metallurgical Engineers 146, 54–62.
- Armah, A.K., Awumbila, M., Clark, S., Dzietror, A., Foster-Smith, R., Porter, R., Young, E.M., 1997. Coping responses and strategies in the coastal zone of south-eastern Ghana: a case study in the Anloga area. In: Evans, S.M., Vanderpuye, C.J., Armah, A.K. (Eds.), The Coastal Zone of West Africa—Problems and Management. Proceeding of an International Seminar 23–28 March 1996. Panshaw Press, Accra, Ghana, pp. 17–27.
- Auken, E., Nebel, L., Sørensen, K., Breiner, M., Pellerin, L., Christensen, N.B., 2002. EMMA—a geophysical training and education tool for electromagnetic modeling and analysis. Journal of Environmental and Engineering Geophysics 7, 57–68.

- Auken, E., Jørgensen, F., Sørensen, K., 2003. Large-scale TEM investigation for groundwater. *Exploration Geophysics* 34, 188–194.
- Awadzi, T.W., 2003. Farmers' response to environmental and socio-economic changes along the south-eastern coast of Ghana. In: Mertz, O., Wadley, R., Christensen, A.E. (Eds.), *Local Land Use Strategies in a Globalizing World: Shaping Sustainable Social and Natural Environments*. Proceedings of the International Conference, August 21–23. Institute of Geography, University of Copenhagen, pp. 189–202.
- Bannerman, R.R., 1994. Appraisal of the limestone aquifer of the Keta Basin, Ghana. In: Suokko, T., Soveri, J. (Eds.), *Future Groundwater Resources at Risk*. International Association for Hydrological Sciences, vol. 222, pp. 315–321.
- Cooper Jr., H.H., 1959. A hypothesis concerning the dynamic balance of fresh water and salt water in a coastal aquifer. *Journal of Geophysical Research* 64, 461–467.
- Danielsen, J.E., Auken, E., Jørgensen, F., Søndergaard, V., Sørensen, K., 2003. The application of TEM in hydrogeophysical surveys. *Journal of Applied Geophysics* 53, 181–198.
- Dickson, K.B., Benneh, G., 2001. *A New Geography of Ghana*. Fourth Impression 2001. Longmans Bk. 170 pp.
- Effersø, F., Auken, E., Sørensen, K.I., 1999. Inversion of band-limited TEM responses. *Geophysical Prospecting* 47, 551–564.
- Fetter, C.W., 1993. *Contaminant Hydrogeology*. Macmillan, New York.
- Fitterman, D.V., Stewart, M.T., 1986. Transient electromagnetic sounding for groundwater. *Geophysics* 51, 995–1005.
- Fountain, D., 1998. Airborne electromagnetic system—50 years of development. *Exploration Geophysics* 29, 1–11.
- Gelting, P., 2004. A hydrogeological and geophysical investigation of the groundwater resources on the Keta Strip, Ghana. MSc. thesis, University of Copenhagen. 121 pp.
- Goldman, M., Tabarovsky, L., Rabinovich, M., 1994. On the influence of 3-D structures in the interpretation of transient electromagnetic sounding data. *Geophysics* 59, 889–901.
- Hubbert, M.K., 1940. The theory of groundwater motion. *Journal of Geology* 48, 785–944.
- Kafri, U., Goldman, M., 2005. The use of the time domain electromagnetic method to delineate saline groundwater in granular and carbonate aquifers and to evaluate their porosity. *Journal of Applied Geophysics* 57, 167–178.
- Kortatsi, B.K., Agyekum, W.A., 1999. Environmental impact assessment of large scale groundwater abstraction in the Keta Strip of the Volta Region of Ghana. Water Research Institute (CSIR). Final report, December 1999. 75 pp.
- Kraft, J.C., Chrzastowski, M.J., Belknap, D.F., Toscano, M.A., Fletcher III, C.H., 1987. The transgressive barrier–lagoon coast of Delaware; morphostratigraphy, sedimentary sequences and responses to relative rise in sea level. In: Pilkey, O.H., Howard, J.D. (Eds.), *Sea-level Fluctuation and Coastal evolution*. Society of Economic Paleontologists and Mineralogists, vol. 41, pp. 129–143.
- McNeill, J.D., 1990. Use of electromagnetic methods for groundwater studies. In: Ward, S.H. (Ed.), *Geotechnical and Environmental Geophysics*, vol. 2. Society of Exploration Geophysicists, pp. 191–218.
- Mills, T., Hoekstra, P., Blohm, M., Evans, L., 1988. Time-domain electromagnetic soundings for mapping sea-water intrusion in Monterey County, California. *Ground Water* 26, 771–782.
- Munkholm, M.S., Auken, E., 1996. Electromagnetic noise contamination on transient electromagnetic soundings in culturally disturbed environments. *Journal of Environmental and Engineering Geophysics* 1, 119–127.
- Ojo, O., 1977. *The Climates of West Africa*. Heinemann, London. 218 pp.
- Reinson, G.E., 1992. Transgressive barrier island and estuarine systems. In: Walker, R.G., James, N.P. (Eds.), *Facies Models; Response to Sea Level Change*. Geological Association of Canada, pp. 179–194.
- Schneider, J.C., Kruse, S.E., 2003. A comparison of controls on freshwater lens morphology of small carbonate and siliciclastic islands: examples from barrier islands in Florida, USA. *Journal of Hydrology* 284, 253–269.
- Sørensen, K.I., Auken, E., 2004. SkyTEM—A new high-resolution helicopter transient electromagnetic system. *Exploration Geophysics* 35, 191–199.
- Spies, B.R., Frischknecht, F.C., 1991. Electromagnetic sounding. In: Nabighian, M.N. (Ed.), *Electromagnetic Methods in Applied Geophysics*, vol. 2. Society of Exploration Geophysicists, pp. 398–402.
- Vacher, H.L., 1978. Hydrogeology of Bermuda: significance of an across-the-island variation in permeability. *Journal of Hydrology* 39, 207–226.
- Vacher, H.L., 1988. Dupuit–Ghyben–Herzberg analysis of strip-island lenses. *Geological Society of America Bulletin* 100, 580–591.